

Article

Residue Char Derived from Microwave-Assisted Pyrolysis of Sludge as Adsorbent for the Removal of Methylene Blue from Aqueous Solutions

Gong Cheng ^{1,†}, Yazhuo Li ^{2,3,†}, Liming Sun ¹, Siyi Luo ⁴, George Z. Kyzas ^{5,*}  and Jie Fu ^{3,*} 

¹ Environmental Engineering Center, Shenzhen Academy of Environmental Sciences, Shenzhen 518001, China; chenggong021@163.com (G.C.); slm0422@163.com (L.S.)

² Department of Environmental Science & Engineering, Fudan University, Shanghai 200438, China; 18210740051@fudan.edu.cn

³ School of Environmental Science and Engineering, Huazhong University of Science and Technology, Wuhan 430074, China

⁴ School of Environmental and Municipal Engineering, Qingdao University of Technology, 11 Fushun Rd., Qingdao 266033, China; luosiyi666@126.com

⁵ Department of Chemistry, International Hellenic University, 65404 Kavala, Greece

* Correspondence: kyzas@chem.ihu.gr (G.Z.K.); jiefu@hust.edu.cn (J.F.); Tel.: +30-2510-462218 (G.Z.K.)

† These two authors equally contributed to this paper.

Received: 19 July 2020; Accepted: 9 August 2020; Published: 13 August 2020



Abstract: Residue char is the main by-product of the microwave-assisted pyrolysis of activated sludge and it has a high content of fixed carbon and porous structure, but little is known about its character as an adsorbent. In this study, residue char of activated sludge with microwave-assisted pyrolysis was used as an adsorbent to absorb methylene blue. The effects of pyrolysis temperature, pyrolysis holding time, contact time, and adsorption temperature on the adsorption ability of residue char were investigated. Kinetics, isotherm, and thermodynamic models were also included to study the adsorption behavior. The results showed that the optimal pyrolysis condition was 15 min and 603 °C, and the adsorption capacity reached up to 80.01 mg/g. The kinetics analyses indicated the adsorption behavior followed the pseudo-second-order kinetics model and the adsorption process was mainly due to chemical interaction. The adsorption isotherm was described by Freundlich model and thus, its process was multimolecular layer adsorption. Furthermore, the thermodynamics parameters (ΔG^0 , ΔH^0 , and ΔS^0) at different temperatures indicated that the nature of the adsorption process was endothermic and spontaneous.

Keywords: sewage sludge; residue char; microwave pyrolysis; adsorption; methylene blue

1. Introduction

In recent years, eliminating dyes from wastewater has attracted great attention [1,2]. Synthetic dyes are widely applied in various industries, including leather, textile, printing, cosmetics, and food processing [3]. The components of dyes are complicated, consisting of aromatic rings and azo and amino groups, which make them toxic, carcinogenic to aquatic life, and difficult to degrade [3]. Methylene blue is considered as one of the most commonly used dyes [4,5]. During recent years, various technologies have been adopted to eliminate dyes from wastewater, such as photocatalysis, advanced oxidation processes, biodegradation, electrochemical removal, and ultrafiltration [6,7]. However, the process of these methods is complex and has high costs, which limit their application in wastewater treatment. Adsorption is thought to be a promising technology, due to its simple treatment process, high efficiency, and wide applicability [8–22].

With the development of urbanization and rapid growth of population, urban sewage is discharged increasingly, meanwhile, the wide application of the activated sludge process making the amount of discharged sludge has increased [23]. There are a variety of hazardous materials that exist in the sludge, such as organic matter, metal ions, and pathogenic microorganisms [24,25]. The disposal of sludge has become a great challenge for society. The application of conventional disposal methods such as landfill, incineration, composting, and sea dumping is restricted, due to their negative influence and potential risk on the environment [26].

Microwave pyrolysis technology as a new method in treating sludge, biomass, and different organic wastes has aroused significant attention, since it has remarkable advantages, including volumetric heating, a substantial increase in product value, less polycyclic aromatic hydrocarbons released than traditional pyrolysis, energy-saving, and cost effectiveness [27,28]. Major research has concentrated on the production of bio-oil and fuel gas [29]. Lin et al. [30] investigated the microwave-assisted catalytic pyrolysis of sewage sludge for bio-oil production and found that bio-oil is mainly formed in the pyrolysis temperature range of 200~400 °C. The higher heating rate (faster pyrolysis rate) both improved the yield and quality of bio-oil. Dominguez et al. [31] found that the gas generated by microwave pyrolysis sludge contains a large amount of H₂ and CO, and the content of aromatic compounds and aliphatic compounds in oil is higher compared with conventional pyrolysis. However, as the main by-product, there are few studies focusing on the residue char, which contains a high content of fixed carbon and complex pore structure. Thus, it is reasonable to use it as an adsorbent [32–37].

Therefore, the main purposes of this study were to (i) examine the adsorption capacity for methylene blue of residue char derived from activated sludge by microwave-assisted pyrolysis; (ii) investigate the influences of pyrolysis temperature, pyrolysis holding time, adsorption temperature, and contact time on the adsorption capacity of residue char; (iii) interpret the underlying mechanism on adsorption behavior using the kinetics, isotherm, and thermodynamics models. This work provided a feasible method for the resource utilization of sewage sludge, and the presented results are helpful to further understand the adsorption capacity of residue char for methylene blue.

2. Materials and Methods

2.1. Preparation of Residue Char

Activated sludge used in the experiment was obtained from Jingzhou municipal wastewater treatment plant. About 1 m³ sludge was dried at 105 °C for 24 h, then, ground until passing 120-mesh for analysis. The filtered sludge was used to produce the residue char using the microwave-assisted pyrolysis apparatus (Figure 1).

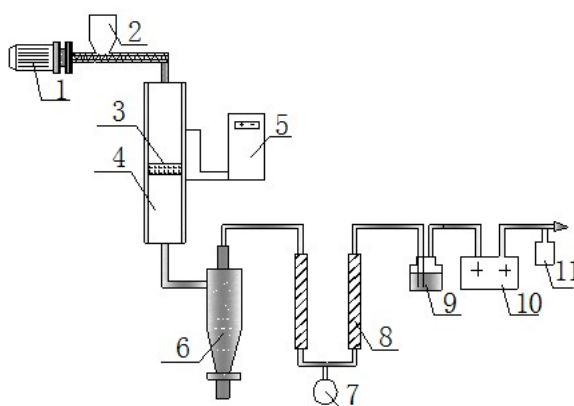


Figure 1. Flowchart of experimental apparatus. (1—motor; 2—hopper; 3—porous ceramic; 4—fixed bed pyrolyzer; 5—temperature controller; 6—cyclone; 7—flask; 8—condenser; 9—silica meter; 10—gas meter; 11—gas sample bag).

Briefly, the dried sludge and the residue char obtained from the last experiment were mixed in a certain proportion, and then, the mixture was put into the sample cell and pyrolyzed at a certain temperature. While the effects of added precursor char quality were not rigorously controlled by this methodology, the precursor char was expected to have a negligible effect on the resultant char. The condensed tar produced by pyrolysis was collected and the non-condensable gases were discharged into the atmosphere. Finally, the residue char in the sample cell was crushed and then, passed through a 120-mesh sieve, and the generated residue char was used for the subsequent adsorption experiment. Table 1 shows the ultimate and proximate analysis of activated sludge. Figure 2 shows the SEM images of the residue char. To investigate the influence of pyrolysis temperatures on the adsorption capacity of the generated residue char, we used the residue char generated at four different temperatures (437, 512, 603, and 700 °C) to conduct the adsorption experiment.

Table 1. Ultimate and proximate analysis of activated sludge.

Ultimate Analysis (%)					Proximate Analysis (%)		
C	H	O	N	S	Volatile matter	Fixed carbon	Ash
19.7	3.2	23.2	3.4	0.5	18.4	38.6	43.1

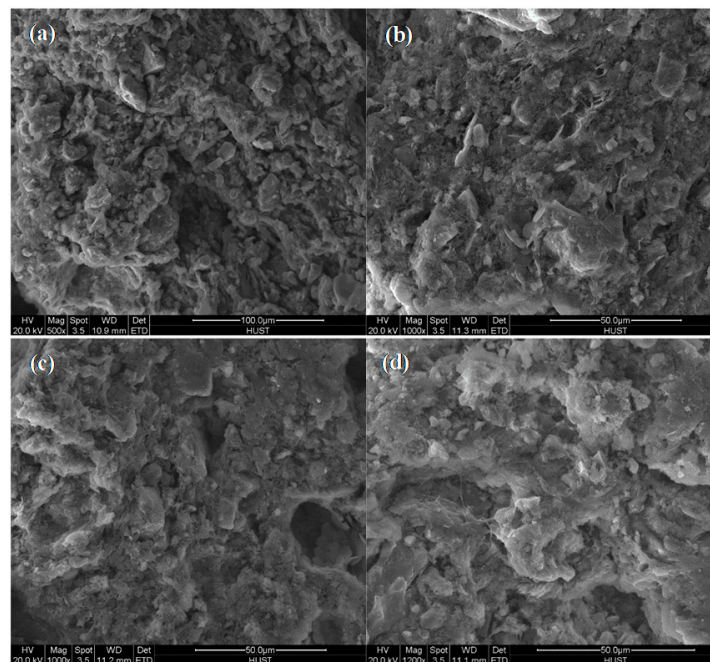


Figure 2. SEM images of residue char. Magnification: 500× (a), 1000× (b,c) and 1200× (d).

2.2. Adsorption Procedures

For the kinetics study, 0.1 g residue char and 100 mL methylene blue solution ($C_0 = 100$ mg/L) were added in a conical flask and then, stirred at 20 °C. Samples were taken at series time intervals, including 15, 30, 45, 60, 90, 120, 180, and 240 min. The concentrations of methylene blue were analyzed using the CARY 50 Prob UV–vis spectrophotometer (Varian, California, United States) at the wavelength of 665 nm. All the experiments were conducted in triplicate to calculate the average value and standard deviation. The adsorption capacity of residue char was calculated by Equation (1):

$$q = \frac{(C_0 - C_t)V}{m} \quad (1)$$

where q (mg/g) is the adsorption capacity; C_0 and C_t (mg/L) are the concentrations of methylene blue at initial and time t , respectively; V (mL) is the volume of solution; m (g) is the weight of adsorbent.

The equilibrium adsorption experiment was performed by adding the 0.1 g of residue char into a series of conical flasks containing 100 mL methylene blue solution of various concentrations (80, 100, 120, and 140 mg/L). The flasks were stirred at 20 °C for 240 min, then, the samples were withdrawn and filtered to measure methylene blue concentrations. Besides, the study was also conducted at 25, 30, 35, and 40 °C to explore adsorption thermodynamics. All the adsorption experiments were conducted in an incubator with a maintained temperature.

2.3. Adsorption Kinetics

The pseudo-first-order, modified pseudo-first-order, and pseudo-second-order kinetics model and the intraparticle diffusion model were used to describe the adsorption kinetics process [38]. The pseudo-first-order kinetic model can be expressed as:

$$\ln(q_e - q_t) = \ln q_e - k_1 t \quad (2)$$

The pseudo-second-order kinetics model can be described as [39–41]:

$$\frac{t}{q_t} = \frac{1}{k_2 q_e^2} + \frac{t}{q_e} \quad (3)$$

The rate constant k_1 of pseudo-first-order kinetics model can be modified as:

$$k_1 = K_1 \frac{q_e}{q_t} \quad (4)$$

Then, the modified pseudo-first-order kinetics model is expressed as:

$$\frac{q_t}{q_e} \ln \left(1 - \frac{q_t}{q_e} \right) = -K_1 t \quad (5)$$

The intraparticle diffusion model is defined by the equation:

$$q_t = k_p t^{0.5} + C \quad (6)$$

where q_e and q_t (mg/g) are the amount of adsorbed methylene blue on residue char at adsorption equilibrium and time t . k_1 (min^{-1}), k_2 ($\text{g} \cdot \text{mg}^{-1} \cdot \text{min}^{-1}$), K_1 (min^{-1}), and k_p ($\text{mg} \cdot \text{g}^{-1} \cdot \text{min}^{-0.5}$) are the rate constants of the pseudo-first-order model, the pseudo-second-order model, the modified pseudo-first-order kinetics model, and the intraparticle diffusion model, respectively [42].

2.4. Adsorption Isotherms

The Langmuir isotherm model assumes that the adsorption of methylene blue on residue char is monolayer and homogeneous; the model can be expressed as follows [43]:

$$\frac{1}{q_e} = \frac{1}{q_m K_L C_e} + \frac{1}{q_m} \quad (7)$$

The Freundlich isotherm model is an experimental model based on the non-ideal and multilayer adsorption on the heterogeneous adsorbent surface, and can be described as [44]:

$$\ln q_e = \ln K_F - \frac{1}{n} \ln C_e \quad (8)$$

where q_e (mg/g) is the adsorbed amount of methylene blue on residue char and q_m (mg/g) is the maximum adsorption amount. C_e (mg/L) is equilibrium concentration. K_L (L/mg) is the Langmuir constant. K_F (L/mg) is the Freundlich constant, representing the adsorption capacity. n is the constant related to the adsorption intensity, and a value of $1/n$ ranging between 0 and 1 indicates the adsorption is favorable [45].

2.5. Adsorption Thermodynamics

Adsorption thermodynamics were used to evaluate the effect of temperature on the adsorption process. The adsorption thermodynamics parameters ΔH^0 , ΔS^0 , and ΔG^0 can be calculated by the following equations:

$$\Delta G^0 = -RT \ln K_C \quad (9)$$

$$\ln K_C = -\frac{\Delta H^0}{RT} + \frac{\Delta S^0}{R} \quad (10)$$

where R (8.314 J/(mol·K)) is the gas constant, K_C is the equilibrium constant at different temperature, T (K) is the temperature, calculated from the intercept of the plot of $\ln(q_e/C_e)$ against q_e . ΔH^0 and ΔS^0 can be calculated from the slope and intercept by plotting $\ln K_C$ against $1/T$ [46].

2.6. The Apparent Adsorption Activation Energy

Supposing that the ΔH^0 and ΔS^0 during the adsorption process are less affected by temperature and can be ignored, the type of adsorption might be determined by the Arrhenius equation [47]:

$$\ln k = -\frac{E_a}{RT} + C \quad (11)$$

where E_a (kJ/mol) is the activation energy, k is the adsorption rate constant, C is the constant, R (8.314 J/mol K) is the ideal gas constant, and T (K) is the temperature.

3. Results and Discussion

3.1. Effect of Pyrolysis Temperature

Pyrolysis temperature plays a critical role in affecting the pore structure and the adsorption property of the residue char. The ideal temperature cannot be reached by directly microwave heating, since most of the components in the activated sludge are not easily heated by microwave [48]. However, the main component of the residue char is fixed carbon, which is good at absorbing microwaves [49]. Salema et al. [50] investigated the effect of char as a microwave absorbent on the microwave pyrolysis of oil palm biomass, and found that the addition of char could improve the heating rate and the microwave pyrolysis products such as bio-oil, char, and gas depends on the proportion of biomass and microwave absorbent. Thus, in this experiment, pyrolysis temperature was changed by adding a certain amount of residue char (5%, 7.5%, 10%, and 12.5%) obtained from the last experiment into the activated sludge.

Figure 3 shows the adsorption capacity for methylene blue of residue char generated under different pyrolysis temperatures. The adsorption capacity increased rapidly from 40.06 mg/g at 240 min to 80.08 mg/g at 120 min with increasing pyrolysis temperature from 437 to 603 °C. This was attributed to the pyrolysis temperature not being high enough to release the volatile matter completely. When the temperature was up to 700 °C, the adsorption capacity decreased.

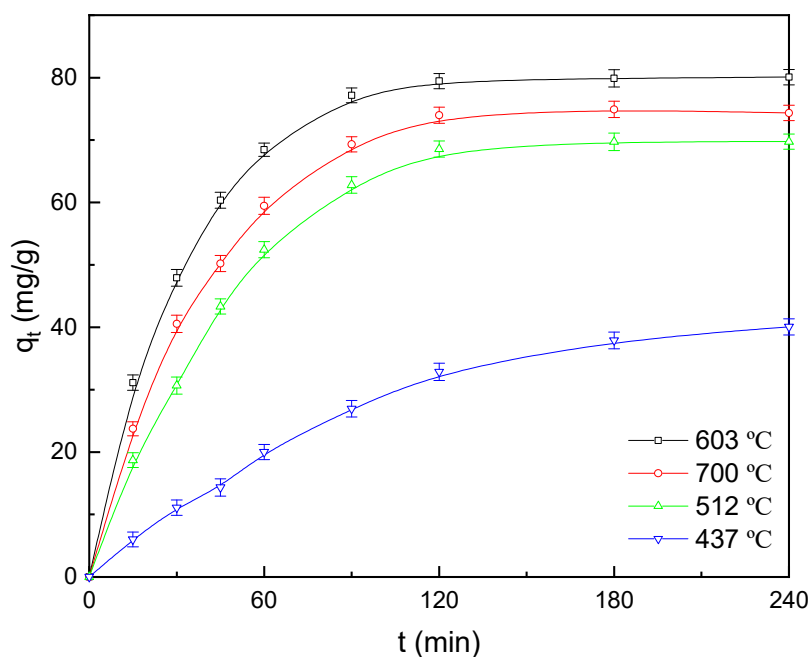


Figure 3. The effect of pyrolysis temperature on adsorption of char.

In previous studies, Chun et al. [51] found that with the temperature increased, the carbonization reaction of residue char became more complete and the porous structure of the char was gradually developed and formed. According to Liu's research, the high carbonization and porous structure of residue char generated under high temperature (603 °C) possessed high chemical stability and large specific surface area, which can provide a great number of adsorption sites for methylene blue [52]. When the temperature rose to 700 °C, the carbon element volatilized and the carbon skeleton structure collapsed, leading to decreased specific surface area and adsorption capacity [53]. Therefore, the pyrolysis temperature had a significant effect on the adsorption capacity of residue char, and higher pyrolysis temperature treatment of residue char can improve its adsorption capacity. To further describe the adsorption process of methylene blue onto residue char, four classical kinetics models were used to simulate the adsorption kinetics. Fitting curves and parameters of kinetics models are shown in Figure 4 and Table 2, respectively. The correlation coefficient indicated that the pseudo-second-order kinetics model could best fit the adsorption process with R^2 ranging from 0.9776 to 0.9952, suggesting the adsorption process for methylene blue on residue char was due to chemical adsorption interaction. Moreover, under the condition of the pseudo-second-order kinetics model, the calculated adsorption capacity of residue char at equilibrium enhanced from 66.67 to 89.29 $\text{mg}\cdot\text{g}^{-1}$ as the pyrolysis temperature rose from 437 to 603 °C. The adsorption rate constant had the same result which increased from 1.05×10^{-4} to 5.24×10^{-4} $\text{g}/(\text{mg}\cdot\text{min})$ with the rising of pyrolysis temperature. These results are consistent with the above result (Figure 3) that elevating pyrolysis temperature was favorable to improve the adsorption capacity of residue char. Franca et al. [54] investigated the ability of coffee press cake treated by microwave pyrolysis for removing methylene blue; when the initial concentration increased from 100 to 750 mg/L , the adsorption capacity increased from 8.7 to 60 mg/g and the rate constant up to 0.0393 $\text{g}\cdot\text{mg}^{-1}\cdot\text{min}^{-1}$. Fan et al. [55] studied the co-pyrolysis of sewage sludge and tea waste for the removal of methylene blue. The maximum rate constant was up to 0.2744 $\text{g}\cdot\text{mg}^{-1}\cdot\text{min}^{-1}$, much higher than the result in this paper, the adsorption capacity only 15 mg/g . Both the adsorption kinetic could be satisfactorily fitted by the pseudo-second-order model, consistent with this paper.

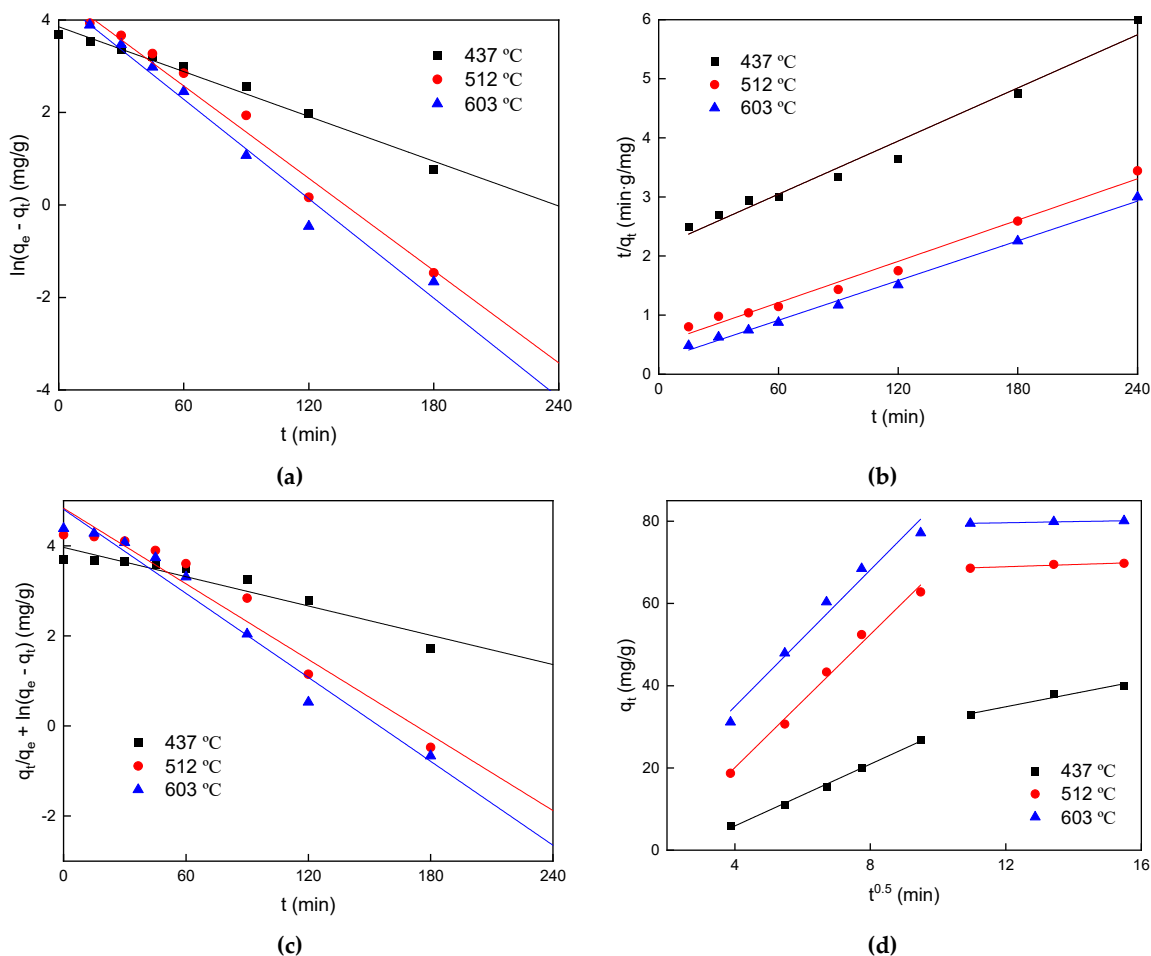


Figure 4. Effect of pyrolysis temperature on adsorption kinetics of char. (a) pseudo-first-order kinetics model; (b) pseudo-second-order kinetics model; (c) modified pseudo-first-order kinetics model; (d) intraparticle diffusion model.

Table 2. Fitting parameters for different kinetics models.

Pyrolysis temperature (°C)	437	512	603	600	600	
Pyrolysis holding time (min)	15	15	15	10	5	
Pseudo-first order kinetics	q_e (mg·g ⁻¹)	47.17	96.66	84.28	69.46	56.49
	k_1 (min ⁻¹)	0.016	0.033	0.035	0.029	0.026
	R^2	0.902	0.980	0.982	0.957	0.960
Pseudo-second order kinetics	q_e (mg·g ⁻¹)	66.67	86.21	89.29	84.75	74.07
	$k_2 \times 10^{-4}$ (g·mg ⁻¹ ·min ⁻¹)	1.05	2.6	5.24	3.89	4.2
	R^2	0.977	0.984	0.995	0.988	0.982
Modified pseudo-first order kinetics	q_e (mg·g ⁻¹)	52.63	125.5	122.3	95.78	77.28
	K_1 (min ⁻¹)	0.010	0.028	0.031	0.024	0.021
	R^2	0.905	0.944	0.969	0.951	0.966
Intraparticle diffusion model	k_{p1} (g·mg ⁻¹ ·min ^{-0.5})	3.758	8.097	9.732	10.08	9.381
	R^2	0.995	0.991	0.996	0.999	0.998
	k_{p2} (g·mg ⁻¹ ·min ^{-0.5})	1.600	0.263	0.426	0.464	0.500
R^2	0.968	0.918	0.698	0.832	0.968	

3.2. Effect of Pyrolysis Time

Figure 5 shows the influence of pyrolysis holding time (5, 10, and 15 min) on the adsorption capacity for methylene blue of residue char. The amount of adsorption of different residue char increased quickly within 120 min and most of the methylene blue was adsorbed in the first 60 min, and the reaction gradually reached the adsorption equilibrium in 240 min. The adsorption capacity (q_e)

of different residue char ranged from 63.14 to 80.08 mg/g, and the adsorption capacity of residue char significantly enhanced with the pyrolysis holding time increasing. It was attributed to the porosity being enhanced and the blocked entrances of pores were cleared at a relatively long retention time [56].

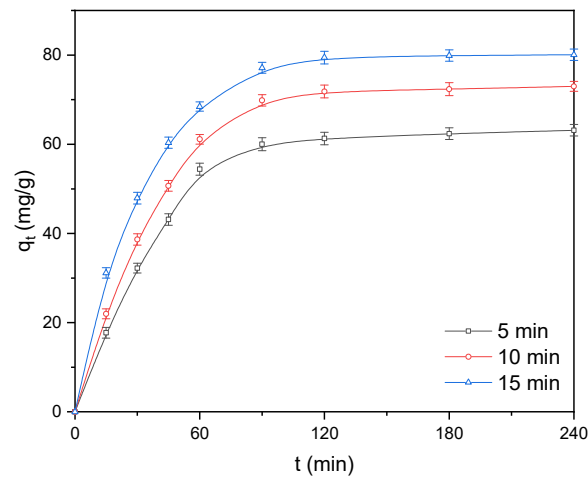


Figure 5. The effect of pyrolysis time on adsorption of char.

Figure 6 presents the kinetic curves about the adsorption of methylene blue onto residue char obtained at different pyrolysis holding times, and the fitting parameters of four kinetics models are listed in Table 2.

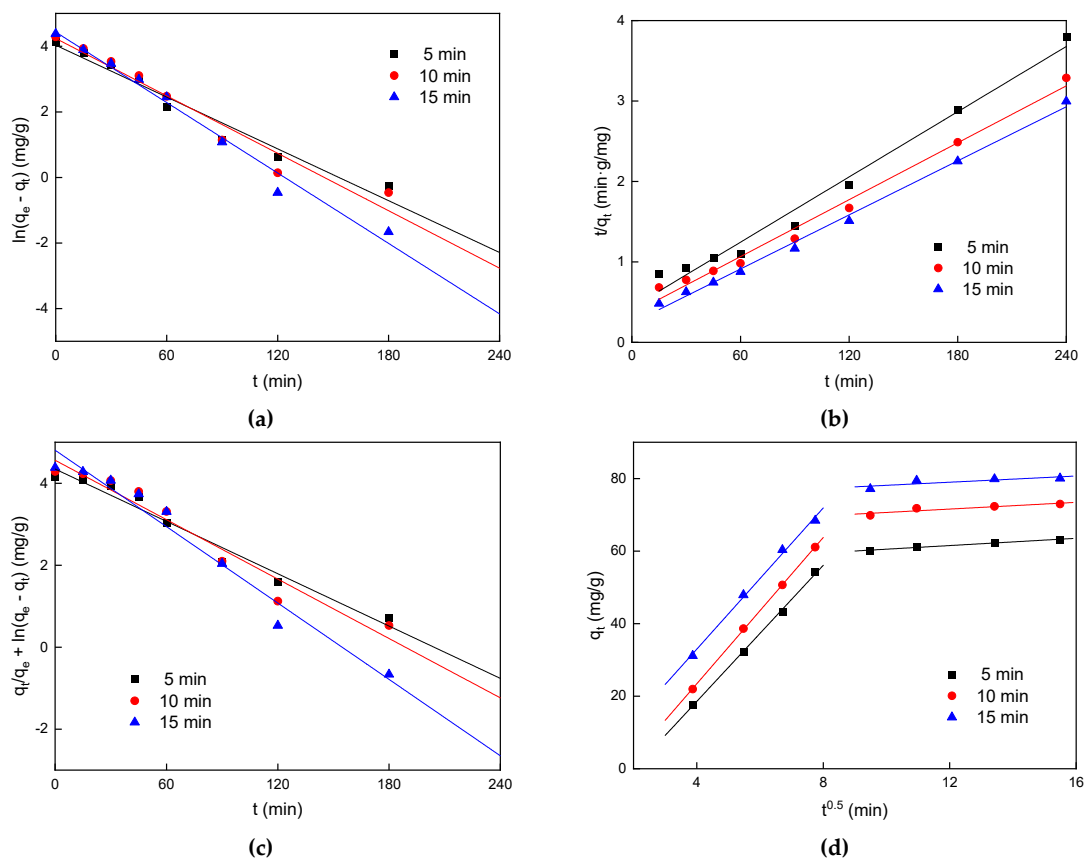


Figure 6. Effect of pyrolysis time on adsorption kinetics of char. (a) pseudo-first-order kinetics model; (b) pseudo-second-order kinetics model; (c) modified pseudo-first-order kinetics model; (d) intraparticle diffusion model.

The pseudo-first-order kinetics equation can describe the initial stage of adsorption well, but as the adsorption process goes on, the measured adsorption data gradually deviated from the fitted curve. Since the pseudo-first-order kinetics model needs to know the q_e before fitting the curves, it is difficult to accurately measure the equilibrium adsorption amount. The correlation coefficient R^2 of the modified pseudo-first-order kinetics model is 0.9517–0.9690. However, the calculated equilibrium adsorption q_e is quite different from the experimental value, indicating that the modified pseudo-first-order kinetics model cannot describe the adsorption process well. In contrast, the pseudo-second-order kinetic model fitted the adsorption process well ($R^2 = 0.9828$ – 0.9952), since the model reflected a comprehensive adsorption mechanism of methylene blue on residue char: the external liquid film diffusion, intraparticle diffusion, and equilibrium adsorption [57].

The intraparticle diffusion model was used to further investigate the adsorption mechanism of methylene blue. The model suggested that if the plot of q_t versus $t^{1/2}$ is linear, the intraparticle diffusion is the main mechanism in this adsorption process [58]. Figure 4d shows a multilinear plot, suggesting the two phases of the methylene blue adsorption on residue char: the initial steep phase and the horizontal phase. The initial rapid phase showed a straight line ($R^2 = 0.9911$ – 0.9998) almost through the origin, which indicated the intraparticle diffusion is the sole rate-limiting step controlling this adsorption process. The fitted curve in the later slow phase ($R^2 = 0.6988$ – 0.9681) showed the adsorption process had reached the equilibrium stage, in addition to intraparticle diffusion, and there were other factors that affect this process [59].

3.3. Equilibrium Isotherms

Figure 7 presents the adsorption isotherms of methylene blue on residue char at different adsorption temperatures (20, 25, 30, 35, and 40 °C) with initial concentrations varying from 80 to 140 mg/L. The adsorption capacity significantly increased with an increase in equilibrium concentrations and the residue char possessed the highest adsorption capacity when the temperature reached 40 °C, which indicated that the improved adsorption temperature could enhance the adsorption ability of residue char.

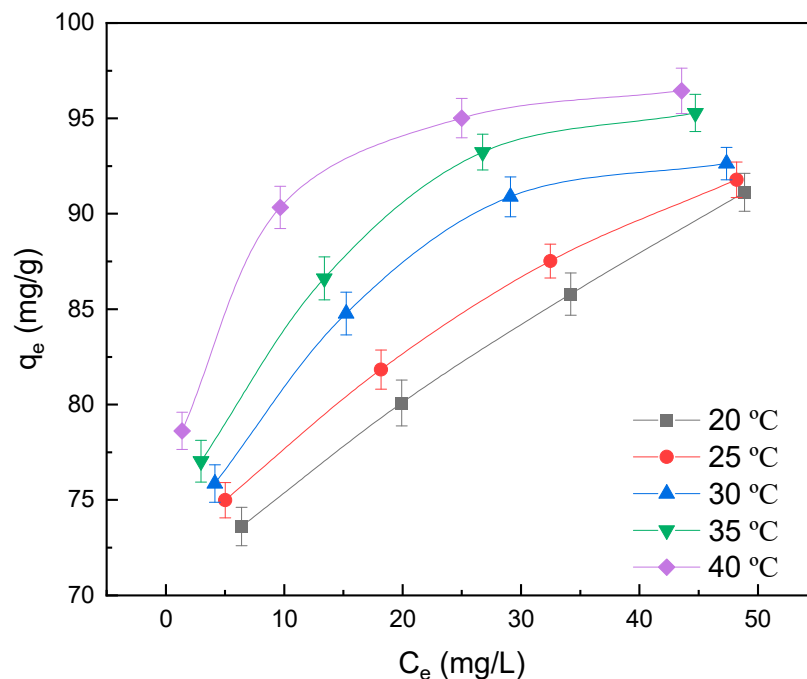


Figure 7. Relationship of equilibrium concentrations and equilibrium adsorption at different temperatures.

The classic Langmuir and Freundlich isotherm models were used to describe the adsorption process, and the fitting curves and parameters are listed in Figure 8. As shown in Table 3, the saturated q_m calculated from the Langmuir model was closer to that obtained from the experiment. However, when the adsorption temperature gradually decreased, the R^2 declined simultaneously, which indicated that the Langmuir model did not fit the isotherm data very well. Conversely, the Freundlich model exhibited a good simulation of the adsorption process with R^2 varying from 0.9625 to 0.9914, which shows that the adsorption is multimolecular layer adsorption [60]. As the adsorption temperature increased, the n and K_F increased, suggesting the residue char had stronger adsorption performance at high adsorption temperature, which was consistent with the result of Figure 7. Besides, the K_F increased with the increment of temperature, suggesting that the adsorption process was endothermic. The $1/n$ values between 0 and 1 showed that the adsorption process was favorable [61].

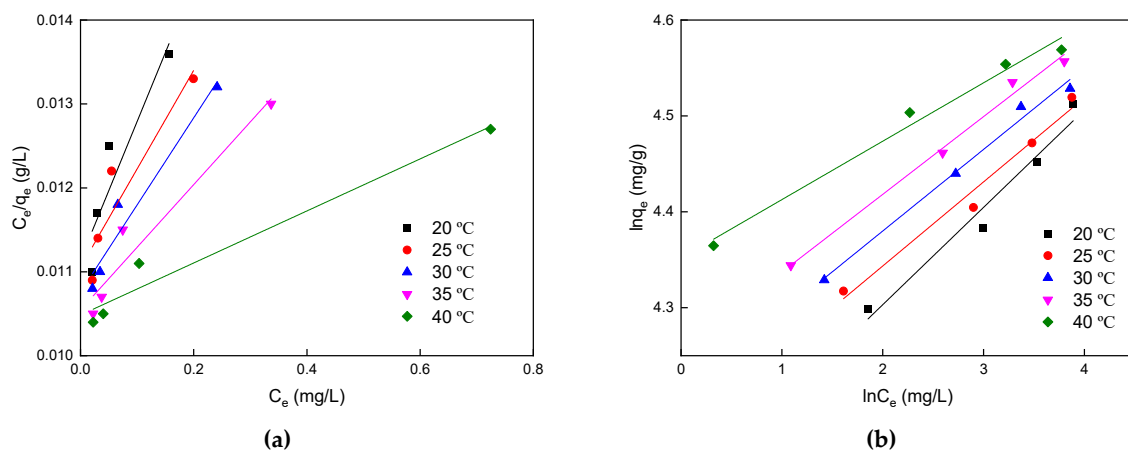


Figure 8. Adsorption isotherms at different temperatures. (a) Langmuir isotherm model; (b) Freundlich isotherm model.

Table 3. Parameters of isotherm models.

Temperature (K)	Langmuir Model			Freundlich Model		
	$q_m/\text{mg}\cdot\text{g}^{-1}$	$K_L/\text{L}\cdot\text{mg}^{-1}$	R^2	K_F	$1/n$	R^2
293	90.09	0.672	0.857	60.3	0.101	0.962
298	90.09	0.948	0.873	64.5	0.087	0.977
303	92.59	1.038	0.949	67.3	0.085	0.989
308	95.24	1.400	0.942	70.5	0.081	0.991
313	95.24	3.387	0.963	77.6	0.060	0.983

3.4. Adsorption Thermodynamics

Figure 9a presents the plot of $\ln K_C$ against $1/T$. The parameters of thermodynamics at different temperatures are listed in Table 4. The negative values of ΔG^0 suggested that the adsorption process was spontaneous [62]. The positive value of ΔH^0 suggested that the adsorption process was endothermic, and the result was confirmed by the fact that q_m increased with increasing temperature [63]. The positive value of ΔS^0 reflects the increased randomness at the solid/liquid interface during the adsorption process [64].

3.5. The Apparent Adsorption Activation Energy

The pseudo-second-order kinetics equation could better describe the adsorption process, thus, the adsorption rate constant k was gained from the pseudo-second-order kinetics model. Figure 9b presents the pseudo-second kinetic fitting curves of the adsorption of methylene blue on residue char under various temperatures at 20, 30, and 40 °C, respectively. The values of R^2 were 0.995, 0.995,

and 0.996, and the values of k were 5.24×10^{-4} , 5.79×10^{-4} , and 6.18×10^{-4} g/(mg·min), respectively. The activation energy was 6.30 kJ/mol, calculated from the slope of $\ln k$ versus $1/T$ shown in Figure 9c [65]. Low activation energies (5–40 kJ/mol) are characteristic of physisorption; higher activation energies (40–800 kJ/mol) indicate the process is chemisorption [66].

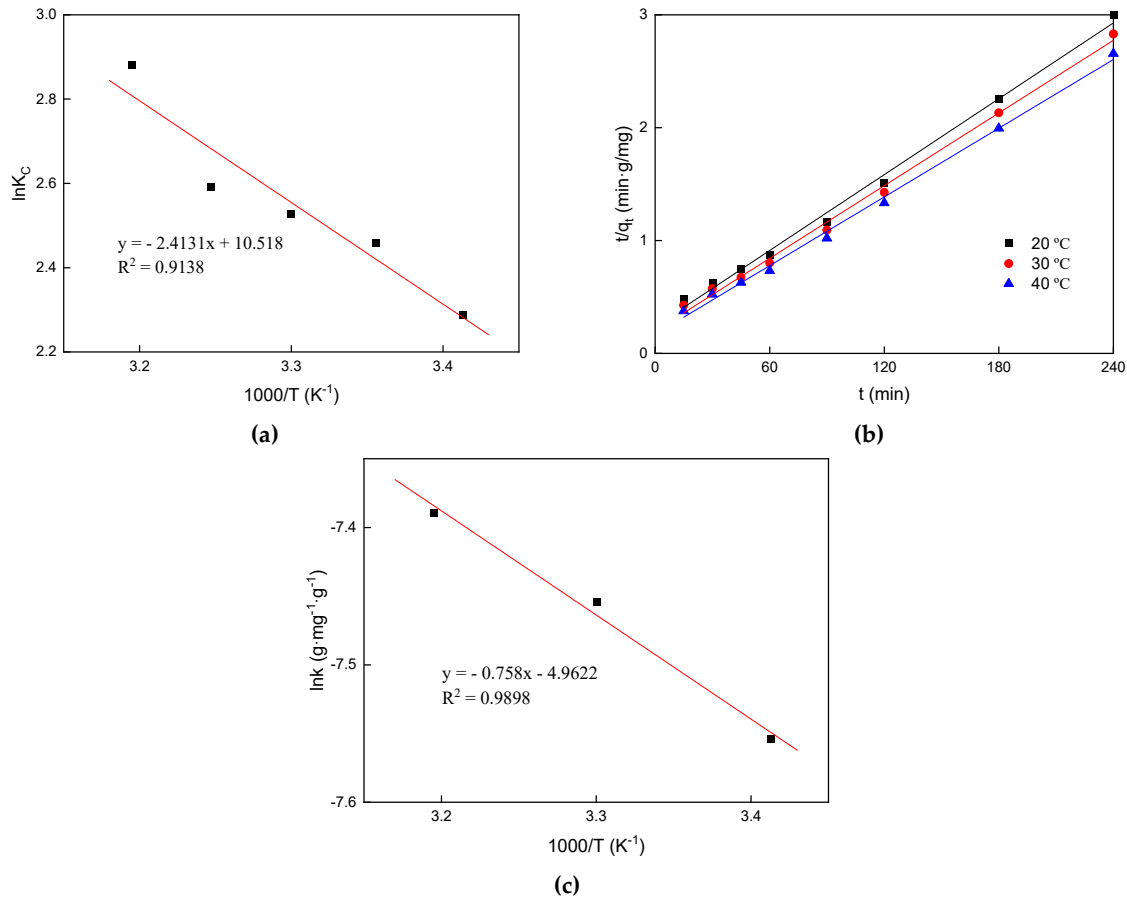


Figure 9. The thermodynamic and activation energy of adsorption. (a) Relationship between $\ln K_C$ and $1/T$; (b) the pseudo-second-order kinetics model; (c) Relationship between $\ln k$ and $1/T$.

Table 4. Thermodynamic parameters at different temperatures.

Temperature (K)	K_C	ΔG^0 (kJ·mol ⁻¹)	ΔS^0 (J·mol ⁻¹ ·K ⁻¹)	ΔH^0 (kJ·mol ⁻¹)
293	9.860	-5.57		
298	11.68	-6.09		
303	12.51	-6.37	87.45	20.30
308	13.33	-6.63		
313	17.85	-7.50		

4. Conclusions

Residue char obtained by microwave-assisted pyrolysis of activated sludge presented a satisfactory result on the adsorption of methylene blue. When the pyrolysis time is 15 min and the pyrolysis temperature is 603 °C, the adsorption amount is up to 80.01 mg/g. The adsorption capacity increased with the increment of pyrolysis temperature and holding time. The adsorption process can be satisfactorily described by the pseudo-second-order kinetic model, which means the adsorption process was mainly due to chemical interaction. The Freundlich model exhibited a good simulation of the adsorption process, with R^2 varying from 0.9625 to 0.9914, suggesting the adsorption was multimolecular layer adsorption. The q_m , k_L , and k_F increased with the increasing adsorption

temperature and the thermodynamic constants ΔG^0 , ΔH^0 , and ΔS^0 were -5.57 (at $20\text{ }^\circ\text{C}$), 20.30 , and 87.45 kJ/mol, respectively, which indicated the process was spontaneous and endothermic. This study provides a theoretical foundation for the resource utilization of activated sludge.

Author Contributions: Conceptualization, G.C. and J.F.; methodology, G.C.; software, L.S.; validation, S.L.; formal analysis, G.C. and Y.L.; writing—original draft preparation, Y.L.; writing—review and editing, G.C., Y.L., G.Z.K. and J.F.; supervision, G.Z.K. and J.F. All authors have read and agree to the published version of the manuscript.

Funding: The project is supported by Major Science and Technology Program for Water Pollution Control and Treatment (2012ZX07206-006), Knowledge Innovation Program of Shenzhen (JCYJ20160526162154729), Qingdao Science and Technology Program (17-3-3-77-nsh), the Key research and development plan of Shandong Province (2018GSF117042), and National Natural Science Foundation of China (41701541).

Conflicts of Interest: The authors declare no conflict of interest.

References

1. Anastopoulos, I.; Hosseini-Bandegharai, A.; Fu, J.; Mitropoulos, A.C.; Kyzas, G.Z. Use of nanoparticles for dye adsorption: Review. *J. Dispers. Sci. Technol.* **2018**, *39*, 836–847. [[CrossRef](#)]
2. Li, Q.; Wang, X.; Xiong, X.; Zhu, S.; Meng, Z.; Hong, Y.; Lin, C.; Liu, X.; Lin, Y. Graphene-supported biomimetic catalysts with synergistic effect of adsorption and degradation for efficient dye capture and removal. *Chin. Chem. Lett.* **2020**, *31*, 239–243. [[CrossRef](#)]
3. Zeng, Q.F.; Fu, J.; Zhou, Y.; Shi, Y.T.; Zhu, H.L. Photooxidation Degradation of Reactive Brilliant Red K-2BP in Aqueous Solution by Ultraviolet Radiation/Sodium Hypochlorite. *CLEAN-Soil Air Water* **2009**, *37*, 574–580. [[CrossRef](#)]
4. Rafatullah, M.; Sulaiman, O.; Hashim, R.; Ahmad, A. Adsorption of methylene blue on low-cost adsorbents: A review. *J. Hazard. Mater.* **2010**, *177*, 70–80. [[CrossRef](#)] [[PubMed](#)]
5. Vadivelan, V.; Kumar, K.V. Equilibrium, kinetics, mechanism, and process design for the sorption of methylene blue onto rice husk. *J. Colloid Interface Sci.* **2005**, *286*, 90–100. [[CrossRef](#)] [[PubMed](#)]
6. Fu, J.; Ding, Y.H.; Ma, G.Y.; Yang, J.; Zeng, Q.F.; Liu, M.Y.; Xia, D.S.; Zhu, H.L.; An, S.Q. Removal of a Toxic Anthraquinone Dye by Combination of Red Mud Coagulation and Ozonation. *Ozone Sci. Eng.* **2009**, *31*, 294–300. [[CrossRef](#)]
7. Lei, X.; Li, X.; Ruan, Z.; Zhang, T.; Pan, F.; Li, Q.; Xia, D.; Fu, J. Adsorption-photocatalytic degradation of dye pollutant in water by graphite oxide grafted titanate nanotubes. *J. Mol. Liq.* **2018**, *266*, 122–131. [[CrossRef](#)]
8. Zhang, X.; Gao, B.; Creamer, A.E.; Cao, C.; Li, Y. Adsorption of VOCs onto engineered carbon materials: A review. *J. Hazard. Mater.* **2017**, *338*, 102–123. [[CrossRef](#)]
9. Camu, E.; Pasten, B.; Matus, C.; Ramirez, F.; Ojeda, J.; Aguila, G.; Baeza, P. Simultaneous adsorption of 4,6-dimethyldibenzothiophene and quinoline over Nickel and Boron modified Gamma-Al₂O₃ adsorbent. *Processes* **2020**, *8*, 419. [[CrossRef](#)]
10. De Carvalho, F.C.; do Nascimento, P.F.; de Souza, M.R.O.; Araujo, A.S. The efficiency of bimodal silica as a carbon dioxide adsorbent for natural gas treatment. *Processes* **2020**, *8*, 289. [[CrossRef](#)]
11. Edet, U.A.; Ifealebuegu, A.O. Kinetics, isotherms, and thermodynamic modeling of the adsorption of phosphates from model wastewater using recycled brick waste. *Processes* **2020**, *8*, 665. [[CrossRef](#)]
12. Ermolenko, A.; Shevelev, A.; Vikulova, M.; Blagova, T.; Altukhov, S.; Gorokhovskiy, A.; Godymchuk, A.; Burmistrov, I.; Offor, P.O. Wastewater treatment from lead and strontium by potassium polytitanates: Kinetic analysis and adsorption mechanism. *Processes* **2020**, *8*, 217. [[CrossRef](#)]
13. Fu, L.; Zhu, J.; Huang, W.; Fang, J.; Sun, X.; Wang, X.; Liao, K. Preparation of nano-porous carbon-silica composites and its adsorption capacity to volatile organic compounds. *Processes* **2020**, *8*, 372. [[CrossRef](#)]
14. Gargiulo, N.; Peluso, A.; Caputo, D. MOF-based adsorbents for atmospheric emission control: A review. *Processes* **2020**, *8*, 613. [[CrossRef](#)]
15. Huang, S.; You, Z.; Jiang, Y.; Zhang, F.; Liu, K.; Liu, Y.; Chen, X.; Lv, Y. Fabrication of ultrathin MoS₂ nanosheets and application on adsorption of organic pollutants and heavy metals. *Processes* **2020**, *8*, 504. [[CrossRef](#)]
16. Inglezakis, V.J.; Balsamo, M.; Montagnaro, F. A fractal-based correlation for time-dependent surface diffusivity in porous adsorbents. *Processes* **2020**, *8*, 689. [[CrossRef](#)]

17. Khamis, M.I.; Ibrahim, T.H.; Jumean, F.H.; Sara, Z.A.; Atallah, B.A. Cyclic sequential removal of alizarin red S Dye and Cr(VI) ions using wool as a low-cost adsorbent. *Processes* **2020**, *8*, 556. [[CrossRef](#)]
18. Khandaker, T.; Hossain, M.S.; Dhar, P.K.; Rahman, M.S.; Hossain, M.A.; Ahmed, M.B. Efficacies of carbon-based adsorbents for carbon dioxide capture. *Processes* **2020**, *8*, 654. [[CrossRef](#)]
19. Marocco, A.; Dell'Agli, G.; Sannino, F.; Esposito, S.; Bonelli, B.; Allia, P.; Tiberto, P.; Barrera, G.; Pansini, M. Removal of agrochemicals from waters by adsorption: A critical comparison among humic-like substances, zeolites, porous oxides, and magnetic nanocomposites. *Processes* **2020**, *8*, 141. [[CrossRef](#)]
20. Qiu, F.; Liu, D.; Cai, Y.; Liu, N.; Qiu, Y. Methane adsorption interpreting with adsorption potential and its controlling factors in various rank coals. *Processes* **2020**, *8*, 390. [[CrossRef](#)]
21. Veclani, D.; Tolazzi, M.; Melchior, A. Molecular interpretation of pharmaceuticals' adsorption on carbon nanomaterials: Theory meets experiments. *Processes* **2020**, *8*, 642. [[CrossRef](#)]
22. Zhang, J.; Deng, R.; Ren, B.; Yaseen, M.; Hursthouse, A. Enhancing the removal of Sb (III) from water: A Fe₃O₄@HCO composite adsorbent caged in sodium alginate microbeads. *Processes* **2020**, *8*, 44. [[CrossRef](#)]
23. Zhang, J.; Zuo, W.; Tian, Y.; Chen, L.; Yin, L.; Zhang, J. Sulfur Transformation during Microwave and Conventional Pyrolysis of Sewage Sludge. *Environ. Sci. Technol.* **2017**, *51*, 709–717. [[CrossRef](#)] [[PubMed](#)]
24. Agrafioti, E.; Bouras, G.; Kalderis, D.; Diamadopoulos, E. Biochar production by sewage sludge pyrolysis. *J. Anal. Appl. Pyrolysis* **2013**, *101*, 72–78. [[CrossRef](#)]
25. Dogru, M.; Midilli, A.; Howarth, C.R. Gasification of sewage sludge using a throated downdraft gasifier and uncertainty analysis. *Fuel Process. Technol.* **2002**, *75*, 55–82. [[CrossRef](#)]
26. Raheem, A.; Sikarwar, V.S.; He, J.; Dastyar, W.; Dionysiou, D.D.; Wang, W.; Zhao, M. Opportunities and challenges in sustainable treatment and resource reuse of sewage sludge: A review. *Chem. Eng. J.* **2018**, *337*, 616–641. [[CrossRef](#)]
27. Motasemi, F.; Afzal, M.T. A review on the microwave-assisted pyrolysis technique. *Renew. Sustain. Energy Rev.* **2013**, *28*, 317–330. [[CrossRef](#)]
28. Zhang, H.; Gao, Z.; Liu, Y.; Ran, C.; Mao, X.; Kang, Q.; Ao, W.; Fu, J.; Li, J.; Liu, G.; et al. Microwave-assisted pyrolysis of textile dyeing sludge, and migration and distribution of heavy metals. *J. Hazard. Mater.* **2018**, *355*, 128–135. [[CrossRef](#)]
29. Chen, Y.R. Microwave pyrolysis of oily sludge with activated carbon. *Environ. Technol.* **2016**, *37*, 3139–3145. [[CrossRef](#)]
30. Lin, Q.; Chen, G.; Liu, Y. Scale-up of microwave heating process for the production of bio-oil from sewage sludge. *J. Anal. Appl. Pyrolysis* **2012**, *94*, 114–119. [[CrossRef](#)]
31. Dominguez, A.; Menendez, J.A.; Inguanzo, M.; Pis, J.J. Production of bio-fuels by high temperature pyrolysis of sewage sludge using conventional and microwave heating. *Bioresour. Technol.* **2006**, *97*, 1185–1193. [[CrossRef](#)] [[PubMed](#)]
32. Chimpae, S.; Wongsakulphasatch, S.; Vivanpatarakij, S.; Glinrun, T.; Wiwatwongwana, F.; Maneeprakorn, W.; Assabumrungrat, S. Syngas production from combined steam gasification of biochar and a sorption-enhanced water-gas shift reaction with the utilization of CO₂. *Processes* **2019**, *7*, 349. [[CrossRef](#)]
33. Liu, L.; Li, Y.; Fan, S. Preparation of KOH and H₃PO₄ modified biochar and its application in methylene blue removal from aqueous solution. *Processes* **2019**, *7*, 891. [[CrossRef](#)]
34. Nicolaou, E.; Philippou, K.; Anastopoulos, I.; Pashalidis, I. Copper adsorption by magnetized pine-needle biochar. *Processes* **2019**, *7*, 903. [[CrossRef](#)]
35. Siddeeg, S.M.; Tahoon, M.A.; Rebah, F.B. Simultaneous removal of calconcarboxylic acid, NH₄⁺ and PO₄³⁻ from pharmaceutical effluent using iron oxide-biochar nanocomposite loaded with *Pseudomonas putida*. *Processes* **2019**, *7*, 800. [[CrossRef](#)]
36. Tsai, W.T.; Hsu, C.H.; Lin, Y.Q.; Tsai, C.H.; Chen, W.S.; Chang, Y.T. Enhancing the pore properties and adsorption performance of cocoa pod husk (CPH)-Derived biochars via post-acid treatment. *Processes* **2020**, *8*, 144. [[CrossRef](#)]
37. Wu, B.; Xi, B.; He, X.; Sun, X.; Li, Q.; Ouche, Q.; Zhang, H.; Xue, C. Methane emission reduction enhanced by hydrophobic biochar-modified soil cover. *Processes* **2020**, *8*, 162. [[CrossRef](#)]
38. Dang, C.; Yang, Z.; Liu, W.; Du, P.; Cui, F.; He, K. Role of extracellular polymeric substances in biosorption of Pb²⁺ by a high metal ion tolerant fungal strain *Aspergillus niger* PTN31. *J. Environ. Chem. Eng.* **2018**, *6*, 2733–2742. [[CrossRef](#)]
39. Ho, Y.S.; McKay, G. Pseudo-second order model for sorption processes. *Process Biochem.* **1999**, *34*, 451–465. [[CrossRef](#)]

40. Ho, Y.S.; Ofomaja, A.E. Pseudo-second-order model for lead ion sorption from aqueous solutions onto palm kernel fiber. *J. Hazard. Mater.* **2006**, *129*, 137–142. [[CrossRef](#)]
41. Ho, Y.S.; Wang, C.C. Pseudo-isotherms for the sorption of cadmium ion onto tree fern. *Process Biochem.* **2004**, *39*, 761–765. [[CrossRef](#)]
42. Nguyen, T.A.H.; Ngo, H.H.; Guo, W.S.; Zhou, J.L.; Wang, J.; Liang, H.; Li, G. Phosphorus elimination from aqueous solution using ‘zirconium loaded okara’ as a biosorbent. *Bioresour. Technol.* **2014**, *170*, 30–37. [[CrossRef](#)] [[PubMed](#)]
43. Xiong, L.; Yang, Y.; Mai, J.; Sun, W.; Zhang, C.; Wei, D.; Chen, Q.; Ni, J. Adsorption behavior of methylene blue onto titanate nanotubes. *Chem. Eng. J.* **2010**, *156*, 313–320. [[CrossRef](#)]
44. Ho, Y. Isotherms for the Sorption of Lead onto Peat: Comparison of Linear and Non-Linear Methods. *Pol. J. Environ. Stud.* **2006**, *15*, 81–86.
45. Mahapatra, K.; Ramteke, D.S.; Paliwal, L.J. Production of activated carbon from sludge of food processing industry under controlled pyrolysis and its application for methylene blue removal. *J. Anal. Appl. Pyrolysis* **2012**, *95*, 79–86. [[CrossRef](#)]
46. Fu, J.; Chen, Z.; Wang, M.; Liu, S.; Zhang, J.; Zhang, J.; Han, R.; Xu, Q. Adsorption of methylene blue by a high-efficiency adsorbent (polydopamine microspheres): Kinetics, isotherm, thermodynamics and mechanism analysis. *Chem. Eng. J.* **2015**, *259*, 53–61. [[CrossRef](#)]
47. Almeida, C.A.P.; Debacher, N.A.; Downs, A.J.; Cottet, L.; Mello, C.A.D. Removal of methylene blue from colored effluents by adsorption on montmorillonite clay. *J. Colloid Interface Sci.* **2009**, *332*, 46–53. [[CrossRef](#)]
48. Peng, F.; He, P.-W.; Luo, Y.; Lu, X.; Liang, Y.; Fu, J. Adsorption of Phosphate by Biomass Char Deriving from Fast Pyrolysis of Biomass Waste. *CLEAN-Soil Air Water* **2012**, *40*, 493–498. [[CrossRef](#)]
49. Ethaib, S. Effects of microwave absorbers on the products of microwave pyrolysis of oily sludge. *J. Eng. Sci. Technol.* **2018**.
50. Salema, A.A.; Ani, F.N. Microwave induced pyrolysis of oil palm biomass. *Bioresour. Technol.* **2011**, *102*, 3388–3395. [[CrossRef](#)]
51. Chun, Y.N.; Kim, S.C.; Yoshikawa, K. Pyrolysis gasification of dried sewage sludge in a combined screw and rotary kiln gasifier. *Appl. Energy* **2011**, *88*, 1105–1112. [[CrossRef](#)]
52. Liu, R.L.; Liu, Y.; Zhou, X.Y.; Zhang, Z.Q.; Zhang, J.; Dang, F.Q. Biomass-derived highly porous functional carbon fabricated by using a free-standing template for efficient removal of methylene blue. *Bioresour. Technol.* **2014**, *154*, 138–147. [[CrossRef](#)] [[PubMed](#)]
53. Ren, X.; Liang, B.; Liu, M.; Xu, X.; Cui, M. Effects of pyrolysis temperature, time and leaf litter and powder coal ash addition on sludge-derived adsorbents for nitrogen oxide. *Bioresour. Technol.* **2012**, *125*, 300–304. [[CrossRef](#)] [[PubMed](#)]
54. Franca, A.S.; Oliveira, L.S.; Nunes, A.A.; Alves, C.C. Microwave assisted thermal treatment of defective coffee beans press cake for the production of adsorbents. *Bioresour. Technol.* **2010**, *101*, 1068–1074. [[CrossRef](#)]
55. Fan, S.S.; Tang, J.; Wang, Y.; Li, H.; Zhang, H.; Tang, J.; Wang, Z.; Li, X.D. Biochar prepared from co-pyrolysis of municipal sewage sludge and tea waste for the adsorption of methylene blue from aqueous solutions: Kinetics, isotherm, thermodynamic and mechanism. *J. Mol. Liq.* **2016**, *220*, 432–441. [[CrossRef](#)]
56. Guo, J.; Lua, A.C. Characterization of chars pyrolyzed from oil palm stones for the preparation of activated carbons. *J. Anal. Appl. Pyrolysis* **1998**, *46*, 113–125. [[CrossRef](#)]
57. Inyang, M.I.; Gao, B.; Yao, Y.; Xue, Y.; Zimmerman, A.; Mosa, A.; Pullammanappallil, P.; Ok, Y.S.; Cao, X. A review of biochar as a low-cost adsorbent for aqueous heavy metal removal. *Crit. Rev. Environ. Sci. Technol.* **2016**, *46*, 406–433. [[CrossRef](#)]
58. Olu-Owolabi, B.I.; Diagboya, P.N.; Adebowale, K.O. Evaluation of pyrene sorption–desorption on tropical soils. *J. Environ. Manag.* **2014**, *137*, 1–9. [[CrossRef](#)]
59. Di Palma, P.R.; Parmigiani, A.; Huber, C.; Guyennon, N.; Viotti, P. Pore-scale simulations of concentration tails in heterogeneous porous media. *J. Contam. Hydrol.* **2017**, *205*, 47–56. [[CrossRef](#)]
60. Módenes, A.N.; Hinterholz, C.L.; Neves, C.V.; Sanderson, K.; Trigueros, D.E.G.; Espinoza-Quiñones, F.R.; Borba, C.E.; Steffen, V.; Scheufele, F.B.; Kroumov, A.D. A new alternative to use soybean hulls on the adsorptive removal of aqueous dyestuff. *Bioresour. Technol. Rep.* **2019**, *6*, 175–182. [[CrossRef](#)]
61. Wong, S.; Yac’cob, N.A.N.; Ngadi, N.; Hassan, O.; Inuwa, I.M. From pollutant to solution of wastewater pollution: Synthesis of activated carbon from textile sludge for dye adsorption. *Chin. J. Chem. Eng.* **2018**, *26*, 870–878. [[CrossRef](#)]

62. Liu, Y. Is the Free Energy Change of Adsorption Correctly Calculated? *J. Chem. Eng. Data* **2009**, *54*, 1981–1985. [[CrossRef](#)]
63. Chang, J.; Ma, J.; Ma, Q.; Zhang, D.; Qiao, N.; Hu, M.; Ma, H. Adsorption of methylene blue onto Fe₃O₄/activated montmorillonite nanocomposite. *Appl. Clay Sci.* **2016**, *119*, 132–140. [[CrossRef](#)]
64. Fu, J.; Song, R.; Mao, W.J.; Wang, Q.; An, S.Q.; Zeng, Q.F.; Zhu, H.L. Adsorption of disperse blue 2BLN by microwave activated red mud. *Environ. Prog. Sustain. Energy* **2011**, *30*, 558–566. [[CrossRef](#)]
65. Doğan, M.; Alkan, M.; Demirbaş, Ö.; Özdemir, Y.; Özmetin, C. Adsorption kinetics of maxilon blue GRL onto sepiolite from aqueous solutions. *Chem. Eng. J.* **2006**, *124*, 89–101. [[CrossRef](#)]
66. Nollet, H.; Roels, M.; Lutgen, P.; Van der Meeren, P.; Verstraete, W. Removal of PCBs from wastewater using fly ash. *Chemosphere* **2003**, *53*, 655–665. [[CrossRef](#)]



© 2020 by the authors. Licensee MDPI, Basel, Switzerland. This article is an open access article distributed under the terms and conditions of the Creative Commons Attribution (CC BY) license (<http://creativecommons.org/licenses/by/4.0/>).